Hindawi
Mathematical Problems in Engineering
Volume 2019, Article ID 7235239, 13 pages
https://doi.org/10.1155/2019/7235239

*Research Article*

# A Signal Recovery Method Based on Bayesian Compressive Sensing

**Hao Zhanjun**[1,2] **Li Beibei**[1] **and Dang Xiaochao**[1,2]

[1]*College of Computer Science and Engineering, Northwest Normal University, Lanzhou 730070, China*
[2]*Gansu Province Internet of Things Engineering Research Center, Lanzhou 730070, China*

Correspondence should be addressed to Li Beibei; 848275034@qq.com

Received 29 October 2018; Accepted 20 January 2019; Published 11 February 2019

Academic Editor: Isabel S. Jesus



In a precise positioning system, weak signal errors caused by the influence of a human body on signal transmission in complex environments are a main cause of the reduced reliability of communication and positioning accuracy. Therefore, eliminating the influence of interference from human crawling waves on signal transmissions in complex environments is an important task in improving positioning systems. To conclude, an experimental environment is designed in this paper and a method using the Ultra-Wideband (UWB) Local Positioning System II (UWB LPS), called Bayesian Compressed Sensing-Crawling Waves (BCS-CW), is proposed to eliminate the impact of crawling waves using Bayesian compressive sensing. First, analyse the transmission law for crawling waves on the human body. Second, Bayesian compressive sensing is used to recover the UWB crawling wave signal. Then, the algorithm is combined with the maximum likelihood estimation and iterative approximation algorithms to determine the label position. Finally, through experimental verification, the positioning accuracy of this method is shown to be greatly improved compared to that of other algorithms.

## 1. Introduction

With the continuous improvement of wireless technologies such as Bluetooth, ZigBee, and Wi-Fi and the rapid development of ad hoc networks and the Internet of Things, wireless networks have attracted increasing attention from academic circles. Location-based services (LBS) are generally considered to be indispensable key technologies [1–4]. Information from a location service is helpful in providing advance warnings, in decision-making and in emergency postprocessing in the network [5]. For example, wireless networks can be applied to provide location service in complex environments such as coal mines, helping to provide advance warnings of possible disasters. When a disaster occurs, such services can identify the best rescue locations for rescue personnel and aid in planning the safest escape route during evacuations. Information from location services can also provide intuitive geographic information, allowing users to make better decisions and improve the user experience. Using a positioning function, wireless networks in usual office environments can help staff easily find the nearest available printer. However, the contribution of location service information to wireless networks extends much further than that. Wireless location information has a wide range of applications in both static networks and mobile networks [6]. Providing better location services is dependent on the underlying location technologies. Therefore, positioning technology plays a decisive role in the further development of wireless network and research to improve positioning technology is particularly important.

The channel model and ranging error model are important foundations for location algorithms and system performance evaluation can provide simulation data for research on ranging and positioning algorithms [7]. However, the existing channel and ranging error models for Time-of-Arrival (TOA) do not consider human positions and do not include the impact of the human body on the channel and ranging accuracy [8]. In TOA ranging, only the transmission time of the line-of-sight channel between a sender and a receiver represents an accurate distance value [9]. Thus, in indoor environment, detecting the correct signal arrival time from the multipath received signal, the TOA estimation algorithm is the biggest challenge for TOA positioning. Evaluating the

performance of a TOA estimation algorithm requires the support of a multipath channel model [10]. Although the IEEE 802.15.4a standard provides multipath channel models for indoor positioning, these models do not consider the impact on signal transmission of human bodies that carry the sensors [11]. According to the principle of electromagnetic wave diffraction, when the front of the waveform reaches an obstacle, its propagation direction will change accordingly. If the surface of the obstacle is relatively smooth and curved, the electromagnetic wave will continue to propagate along the surface of the obstacle. This mode of propagation is called a crawling wave [12]. Existing research results show that the curved surfaces of the human body cause crawling wave phenomena [13]. Although the human body has a strong shielding effect on the direct-view signal, human crawling waves allow partially obstructed signals to still reach the receiver [14]. The combined effect of human crawling waves and multipath effects will cause change in the number of received signal paths, signal arrival times, and signal energy, which can all affect the accuracy of TOA measurements [15]. When a UWB signal propagates around a human body, the UWB signal's direct path is undetectable due to the human body's occlusion and the UWB channel characteristics are affected by the complex radio wave environment. Thus, a UWB channel model in the human body occlusion scenario differs from the general application model: the UWB channel model in the human body occlusion scenario is much more complex [16]. Therefore, selecting reasonable measurement methods, scene variables, and data analysis methods is indispensable for modelling TOA ranging errors in human occlusion application scenarios.

Current UWB positioning is generally divided into Line-of-Sight (LOS) and Non-Line-of-Sight (NLOS) cases, and most are based on AOA estimation. If the base stations were able to perform both TOA estimation and Direction-of-Arrival (DOA) estimation at the same time, only one base station would be needed for positioning. Previous studies [18–20] have proposed UWB positioning methods based on TOA-DOA joint estimation. In [18], the authors proposed a three-step joint estimation algorithm that first used the threshold correlation method to perform TOA estimation and then used the least mean square algorithm to perform joint estimation of the TOA and DOA time difference. Finally, by increasing the wave estimation accuracy, the time difference is obtained by the DOA estimation. In [19], another three-step joint estimation algorithm was proposed. First, the maximum likelihood estimation algorithm was used to perform the preliminary TOA estimation; then, a further joint estimation of the TOA and the arrival time difference was conducted. Finally, the DOA estimation was acquired using the time difference of arrival (TODA) and the geometric trigonometric cosine theorem. The study in [20] proposes a two-step joint estimation algorithm that uses the TC algorithm to perform a rough estimate of the TOA and then uses a log-likelihood equation to obtain the maximum value. To improve the estimation accuracy of TOA and perform DOA estimation, the algorithm design of [18, 19] requires three steps. While these algorithms are more complex the estimation accuracy of the algorithm in [20] is limited by the sampling frequency; the sampling frequency is in GHz. The Nyquist rate and the system complexity are higher. The approach proposed that this paper eliminates the effect of the synchronization clock through the improved Kalman filter algorithm. We conduct a large number of experiments to verify the method's performance. The main contributions of this paper are as follows:

(1) The classical Saleh–Valenzuela channel approach models the channel impulse response. The method achieves reliable channel estimation and provides an effective UWB channel model.

(2) We perform three-dimensional modelling of the human body to identify the crawling waves generated when signals propagate on the surface of a human body and study the causes and propagation rules of the crawling waves. We weaken the effects of crawling waves on signal propagation through the envelope detection method and the synchronous product detection method. Then, we study the processed crawling wave signal and spectral density to provide a theoretical basis for the Bayesian compressive sensing recovery signal model.

(3) Bayesian compressive sensing restores the UWB signals affected by the human body and combines maximum likelihood estimation with iterative approximation to determine the label position. The feasibility of this method is verified by analysing the signal and spectral density after modulation and demodulation.

(4) We provide thorough experimental verification of the proposed algorithm's performance in a real environment. The article algorithm effectively eliminates the effect of human occlusion on positioning accuracy. We compare the proposed algorithm with existing algorithms to demonstrate that our algorithm performs better.

The remainder of this paper is structured as follows: Section 2 details the related work of the system used in this study. Section 3 describes the algorithm design. Section 4 presents the experiments and an analysis, and Section 5 provides conclusions and future work.

## 2. Related Work

*2.1. UWB Signal Model.* In the classical Saleh–Valenzuela channel model, multipath components arrive in a cluster and the arrival time of rays in a cluster follows a Poisson distribution. The channel impulse response can be modelled as follows:

$$h(t) = \sum_{l=1}^{L} \sum_{k=1}^{K} \alpha_{kl} \delta\left(t - T_l - \tau_{kl}\right) \tag{1}$$

where $\alpha_{kl}$ represents the gain coefficient of the $k$ path of the $l$th cluster, $\delta(t)$ is the Dirac trigonometric function, $\tau_{kl}$ is the delay of the $k$th multipath with respect to the arrival time $T_l$ of the $l$th cluster, $L$ is the number of clusters, and $K$ is the number of multipath in the cluster. In addition, $|\alpha_{kl}|$ follows a lognormal distribution. Due to prior knowledge of channel statistics, we can design a more effective channel estimation algorithm. Figure 1 shows the power delay distribution of the Saleh–Valenzuela channel model. The channel

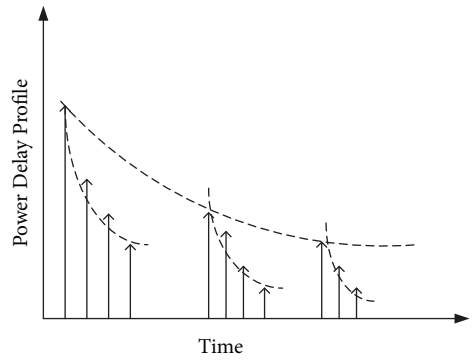


Figure 1: Saleh–Valenzuela channel model.

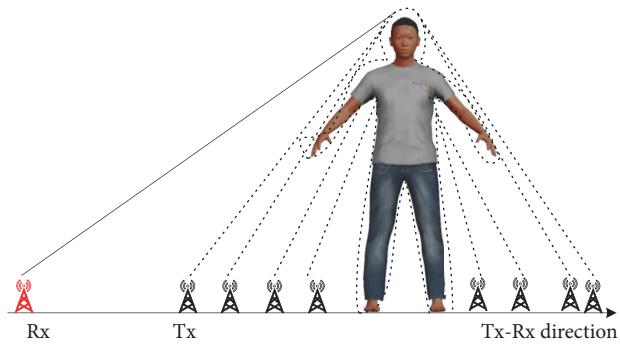


Figure 2: Signal propagation path in a human-occluded application scenario.

follows multipath branches to the receiver, the amplitude is exponentially distributed within the cluster, and there is an attenuation trend between clusters.

*2.2. Crawling Wave Generation.* Human body occlusion is a special scenario in non-line-of-sight (NLOS) propagation. Under human body occlusion, when the transmitting antenna and the receiving antenna are both on the same side of the human body, they are not blocked and pass directly through each other during propagation. Thus, signal path energy loss detection can accurately obtain the direct path signal [19]. However, when the transmitting antenna and the receiving antenna are on different sides of the human body, they are blocked and the energy loss of the direct-path signal cannot be determined from the energy loss of the multipath signal; therefore, the direct-path signal cannot be detected [20]. A large number of research results have shown under human occlusion wireless signals form diffracted waves on the surface of the human body, resulting in reflected and scattered waves from objects around the human body. The radio waves in the channel consist mainly of the above three forms in the channel during propagation [21]. According to the principle of electromagnetic wave diffraction, when the leading edge of a waveform of a radio wave reaches an obstacle, its propagation direction also changes [22]. Because the surface of the human body is smooth and curved, a surface crawling wave forms when the wireless signal propagates on a human body [3]. Despite the strong shielding effect of the human body on the direct-path signal, the surface crawling wave results in a partially occluded wireless signal through propagation on the human body surface; thus, the wireless signal still reaches the receiving antenna. However, the number of signal paths, signal arrival time, and signal energy attenuation all undergo changes that affect the accuracy of TOA ranging results [23]. Therefore, for applications in the presence of human occlusion, the surface crawling wave is the most critical factor affecting wireless signal propagation and TOA ranging. An analysis of the surface crawling wave can help to model the TOA ranging error in the human occlusion application scenario and provide a theoretical basis.

Figure 2 depicts the propagation process of wireless signals in a human occlusion application scenario [24]. The wireless signal is emitted by the transmitting antenna Tx, impacts the human, and then crawls from one side to the other along the surface of the human body, finally reaching the receiving antenna Rx through propagation in the air. As shown in Figure 1, when the transmitting antenna moves from the T1 position to the T4 position, the distance between

the transmitting and the receiving antennae continuously decreases and the wireless signal crawling distance on the human body surface increases and finally propagates through the air. The distance travelled also decreases. According to the distance-based UWB human body propagation model proposed in [25], when the wireless signal propagates on the human body surface, the signal energy per unit distance attenuates faster than that of signal energy propagated in the air. Figure 2 shows that when the transmitting antenna and the receiving antenna are in the vicinity of the human body, the signal energy attenuation mainly occurs because of the path loss caused by the body surface crawling wave. As the transmitting antenna gradually moves away from the human body, the signal energy attenuation path loss mainly occurs from air propagation [26, 27]. Therefore, there is a critical point between the human body and the antenna for waves under human occlusion. The location of this critical point is the main cause of signal energy attenuation [28, 29]. Because the path loss caused by surface crawling waves is larger than the path loss of wireless signals transmitted through the air, the surface crawling waves cause larger TOA ranging errors [30, 31]. Therefore, under human occlusion, the position of the critical point between the human body and the antenna also determines the size of the TOA ranging error and is the main reason for its occurrence.

*2.3. Bayesian Compressed Sensing Model.* A real signal $x \in R^{N\times 1}$ can be represented by a weight coefficient $\varphi_{N*N}$, which can be expressed on a $\theta$ basis as follows:

$$x = \sum_{i=1}^{N} \theta_i \varphi_i \quad \text{i.e. } x = \varphi\theta \tag{2}$$

where $x$ and $\theta$ are all $N \times 1$-order three-dimensional vectors and $\varphi = [\varphi_1, \varphi_2, \varphi_3, \ldots, \varphi_N]$ and $\theta = [\theta_1, \theta_2, \theta_3, \ldots, \theta_N]^T$ are vectors containing $K$ nonzero coefficients. We can express the canonical form of $l_p$ as $\|\cdot\|_p$ and $\theta$ as a sparse signal of size $K$ if $\theta$ satisfies $\|\theta\|_0 \le K$. Then, the compressed measurement sequence $y$ can be obtained by using the linear measurement of the measurement matrix $\phi \in R^{M\times N}$ $(M < N)$, as shown in

$$y = \phi x = \phi\varphi\theta \tag{3}$$

where $\phi$ is the $M \times N$-order matrix representing the sample system and $\phi\varphi$ is defined as the compressed sensing matrix in the compressed sensing problem.

The process of recovering x from the measurement sequence y is called sparse reconstruction. However, this model is an NP-hard problem. Nevertheless, Chen and Candes [31] showed that when the matrix $\phi\varphi$ satisfies certain restricted isometric properties (RIP) with high probability, the reconstruction model can be solved as a linear programming problem, expressed as follows:

$$\begin{aligned} \hat{\theta} &= \arg\min \quad \|\theta\|_1 \\ &\text{s.t.} \quad y = \phi\varphi\theta \end{aligned} \tag{4}$$

In the above formula, when $\phi$ and $\varphi$ are unrelated, $\phi\varphi$ has a high probability of satisfying the RIP. In general, the randomly generated measurement matrix $\phi$ is not related to any fixed matrix $\varphi$. In this paper, we use the Bernoulli random matrix for $\phi$.

In the standard CS framework, the signal reconstruction problem is mainly solved by convex optimization methods such as basic tracking (BP) and greedy algorithms such as matching pursuit (MP) and orthogonal matching pursuit (OMP).

Compression sensing is used to recover the signal through a small number of measurements, and compression sensing can accurately restore the original signal when it is sparse. In other words, after the influence of human body occlusion, the original propagation signal can still be accurately restored. The compressed-sensing signal model is similar to the traditional signal model. Assuming that a is the signal to be perceived, the perceptual process of this signal is described by

$$b = Aa \tag{5}$$

where $a \in R^n$ is the original signal to be perceived, A is an $m \times n$-dimensional measurement matrix, and $b \in R^m$ is the resulting measurement signal. According to the previous signal sampling model, $m \ge n$; however, because m can be much smaller than n when the original signal is sparse, the original signal can also be accurately recovered. In addition, the compressed sensing measurement matrix is randomly generated, effectively avoiding measurement errors. Thus, for a k-dimensional sparse signal, the randomly measured $m$ needs to satisfy the following conditions:

$$m = O\left(k \log\left(\frac{n}{k}\right)\right) \tag{6}$$

Based on the above theoretical description, sparse representation is used in this paper to represent the signal. The sparsity here involves our understanding of the signal transmission strength. The sparse definition derived from mathematical experience is that a vector contains at most k non-zero sparse elements and is calculated by the k-norm, defined as follows.

*Definition 1.* A vector is called k sparse signal if

$$\|x\|_0 = \#\{i : x_i \ne 0\} \le k \tag{7}$$

All the k sparse vector geometries are represented as $\sum_k$; however, combining this with the actual expression is not conducive to calculation. Therefore, we derive Definition 2 to define the best approximation of the k-dimensional sparse vector.

*Definition 2.* Assuming that $1 \le p < +\infty$ and $r > 0$, a signal under a constant C and attenuation index r vector $x = (x_i)_{i=1}^n \in R^n$ is called a $p-$compressible signal if

$$\sigma(x)_p := \min_{x\in\sum_k} \left\|x - \tilde{x}\right\|_p \le C \cdot k^{-r} \tag{8}$$

Then, for any $k \in \{1, \ldots, n\}$, the next signal is the structurally sparse signal. The nonzero sparsity of sparse

signals generally does not randomly appear at any given signal position; instead, their patterns are structural. For example, the main coefficient of a nonzero discrete cosine transform (DCT) coefficient of an image is concentrated in a given part; the other part can be its wavelet decomposition form, which can be shown as a tree structure, defined as follows.

*Definition 3.* Let $\Lambda \subset \{1, \ldots, n\}$, $\delta > 0$, and vector $x = (x_i)_{i=1}^n \in R^n$ be called $\delta$−-related sparse vectors if

$$\left\| 1_\Lambda \subset x \right\|_1 \leq \delta \tag{9}$$

The k-sparse signal can be considered more extensive, while the structure sparsity is based on the signal structure plus some other structural. Let $x \in R^n$ be a k-sparse signal that belongs to the linear subtree of all signals with the same support set space; then, set $\sum_k$ is a set of subspaces where vector $\Lambda$ satisfies $|\Lambda| \leq k$. The natural definition proposed in [3] is as follows.

*Definition 4.* Vector $x \in R^n$ belongs to a set of subspaces when a cluster of subspaces $(W_j)_{j=1}^N \in R^n$ exists such that

$$x \in \bigcup_{j=1}^{N} W_j \tag{10}$$

At the same time, a sparse fusion frame concept was also proposed in [24]. The fusion framework is also a set of subspaces whose signals have the nature of a framework. Signal $(W_j)_{j=1}^N \in R^n$ is a fusion framework within the boundaries A and B if

$$A \|x\|_2^2 \leq \sum_{j=1}^{N} \left\| P w_j(x) \right\|_2^2 \leq bb \|x\|_2^2 \in R^n \tag{11}$$

where $Pw_j$ is the orthogonal projection in subspace $w_j$. The fusion frame theory extends the traditional frame theory. It can be proposed that the structure method is not a subspace extension by analysing the sparse fusion frame theory when the signal is projected in an arbitrary-dimensional subspace.

## 3. Algorithm Design

*3.1. BCS-CW Algorithm.* Based on statistical information of the measurement signal, prior knowledge of the signal in the sparse domain and CS is represented in the Bayesian framework. Compression measurements should also consider measurement noise and additional noise, expressed as follows:

$$y = \phi \varphi^T x + \varepsilon = \phi\theta + \varepsilon \tag{12}$$

where $\varepsilon = [\varepsilon_1, \varepsilon_2, \varepsilon_3, \ldots, \varepsilon_N]$ is an error vector containing measurement noise and additional noise. The error vector $\varepsilon$ is generally modelled as an independent zero-mean Gaussian distribution with a variance of $\sigma_0^2$. If it is defined as $\varepsilon N(0, \sigma_0^2)$, a Gaussian likelihood model is obtained:

$$p\left(y \mid \theta, \sigma_0^2\right) = \left(2\pi\sigma_0^2\right)^{-K/2} \exp\left(-\frac{1}{2\sigma_0^2} \left\| y - \phi\theta^2 \right\|\right) \tag{13}$$

As mentioned above, the coefficients are sparsely constrained. The previously widely used sparsity is the Laplacian density function:

$$p(\theta, \lambda) = \left(\frac{\lambda}{2}\right)^N \exp\left(-\lambda \sum_{i=1}^{N} \theta_i\right) \tag{14}$$

Therefore, the solution in (14) corresponds to the prior maximum a posteriori in (13).

However, the Laplacian prior is not conjugate with Gaussian likelihood, and the associated Bayesian inference may not be performed in closed form. An associated vector machine (RVM) has been applied that has similar properties to the Laplacian prior but allows convenient conjugate index analysis. Thus, zero-mean Gaussian priors are considered for each element of $\theta$:

$$p(\theta \mid \alpha) = \prod_{n=1}^{N} N\left(\theta_n \mid 0, \sigma_n^2\right) \tag{15}$$

where $\alpha = [\alpha_1, \alpha_2, \alpha_3, \ldots, \alpha_N]$ is the accuracy (antivariance) of the Gaussian density function, giving priority to $\alpha$:

$$p(\alpha \mid a, b) = \prod_{n=1}^{N} \Gamma\left(\alpha_n \mid a, b\right) \tag{16}$$

By marginalizing the hyperparameter $\alpha$, the overall a priori value on $\theta$ is

$$p(\alpha \mid a, b) = \prod_{i=1}^{N} \int_0^\infty N\left(\theta_i \mid \alpha_i^{-1}\right) \Gamma\left(\alpha_i \mid a, b\right) d\alpha_i \tag{17}$$

Based on the above discussion, the Bayesian linear model considered on the RVM is essentially a simplified model for Bayesian model selection. We can express the posterior of $\theta$ as a Gaussian distribution whose mean and variance are given by

$$\mu = \alpha_0 \sum \phi^T y \qquad \sum = \left(\alpha_0 \phi^T \phi + A\right)^{-1} \tag{18}$$

where $\alpha_0 = 1/\sigma_0^2$ and $A = \mathrm{diag}[\alpha_1, \alpha_2, \ldots, \alpha_N]$. If we already know these parameters of $\theta$, we can use the posterior mean as an estimate of $\{\alpha_0, \alpha\}$. To estimate the

above parameters, the equivalent of maximizing the marginal probability of E is

$$L(\alpha_0, \alpha) = -\frac{1}{2}\left[K\log(2\pi) + \log|C| + y^T C^{-1} y\right] \quad (19)$$

In the above formula, $C = \sigma_0^2 I + \phi A^{-1}\phi^T$. The point estimate for A uses the Type 2 Maximum Likelihood (ML) method; thus, it results in the following iterative update rules:

$$\alpha_0^{new} = \frac{K - \sum_{i=1}^{N}\gamma_i}{\|y - \phi\mu\|_2^2}$$
$$\alpha_i^{new} = \frac{\gamma_i}{\mu_i^2}, \quad (20)$$
$$i \in \{1, 2, 3, \ldots, N\}$$

where $\mu_i$ is the $i$th element of $\mu$ in (14), $\gamma_i = 1 - \alpha_i \sum_{ii}$, $\sum_{ii}$ is the $i$th diagonal element of $\sum$ in (14), and $K$ is the measured length $y$. The parameters $\{\alpha_0, \alpha\}$ can be obtained after multiple iterations and then used to calculate $\mu$.

*3.2. Bayesian Compressed Sensing Recovers UWB Signals.* To solve the signal compression sensing recovery problem, commonly used effective solutions include greedy iterative algorithms, nonconvex optimization-based iterative algorithms, convex optimization algorithms, and graph theory-based information transfer algorithms. Considering the propagation characteristics of UWB signals under human occlusion, for this study, we chose a simple and effective greedy algorithm.

The greedy algorithm solves the problem iteratively. The core idea is to find the relevant columns of measurement matrix A using a greedy approach and then find the corresponding sparse solution. In each iteration, the algorithm selects a column in the measurement matrix related to y and minimizes the mean square error at each step. Then, the corresponding row contribution subtracts the remaining residual from $y$, which generally requires m iterations. The termination criteria for algorithms generally differ. Most of the iterative algorithms are derived from matching pursuits (Matching Pursuits, MP) and Orthogonal Matching Pursuits (OMP). The greedy algorithm generally has low computational requirements in sparse conditions that increase with the complexity. However, the signal in this case is not particularly sparse, but that means that the signal recovery becomes more complex. In this case, we combine the Bayesian method and the greedy iterative method. The execution steps for the Orthogonal Matching Pursuit (OMP) algorithm are listed below.

*Step 1.* Input measurement matrix A, measurement y, and the error threshold $\sigma$.

*Step 2.* Set k = 0, initialize ${x_{UWB}}^0 = 0$, initialize the residual $r^0 = y - A{x_{UWB}}^0$, and obtain the support set $S0 = \sup px0 = \varnothing$.

*Step 3.* Let k = k + 1 and select $i_0$ for all i so that $\min_c \|ca_{i0} - r^{k-1}\|_2 \le \min_c \|ca_i - r^{k-1}\|_2$, $S^k = S^{k-1} \cup \{i_0\}$;

*Step 4.* As calculated by Step 3 ${x_{UWB}}^k = \min_{x_{UWB}} \|Ax_{UWB} - y\|_2$, in fact $x_{UWB} = S^k$;

*Step 5.* Calculate the residual $r^k = y - A{x_{UWB}}^k$ from Step 4.

*Step 6.* If $\|r^k\|_2 \ge \sigma$ then output the value of the recovered signal ${x_{UWB}}^k$; otherwise, return to Step 2.

The above algorithm provides a basic definition of the OMP algorithm.

*Definition 5.* The measurement matrix $m * n$ is one dimension; let $x_{UWB} \in R^n$ be the solution of the P0 problem and satisfy

$$\|x_{UWB}\|_0 < \frac{1}{2}\left(1 + \mu(A)^{-1}\right) \quad (21)$$

Then, the OMP algorithm can completely recover the UWB signal $x_{UWB}$.

For the OMP algorithm, when one of the following two conditions is met:

(a) The mutual relationship number satisfies A $\mu(A) < 1/(2M - 1)$,

(b) The measurement matrix A satisfies the M+1-order RIP condition, where the constant $\delta_{k+1}$ is satisfied.

Then, the OMP algorithm will completely recover the k sparse signal from $y = Ax_{UWB}$ after k iterations. If the elements of the measurement matrix A are taken independently from the Gaussian distribution, then the OMP will recover the original value with a high probability at the measurement number $O(k \log n)$ of the UWB signal.

## 4. Performance Testing and Analysis

*4.1. Implementation Method*

*4.1.1. Experimental Environment.* For this study, we conducted experiments in both indoor and outdoor environments and included a laboratory, a Meeting-Room, and a corridor. The outdoor environments included a soccer field and an area outside a school building. For each venue, we placed laptops in more than 10 places and placed tags in several different locations. During the experiment, one or more people moved within the environment, for example, students walking on the football field or in the research lab. Diagrams of the experimental environments are shown in Figures 3 and 4.

*4.1.2. Hardware Test Environment.* The hardware system used in this paper is the I-UWB LPS positioning system. At present, the system has achieved 5cm positioning accuracy for a single-label. Figure 5(a) shows the positioning of the base station module and the tag; Figure 5(b) shows the power supply module; Figure 5(c) shows a network diagram of the nodes where the middle tag passes the positioning among the four base stations; and Figure 5(d) shows the serial port communication interface.

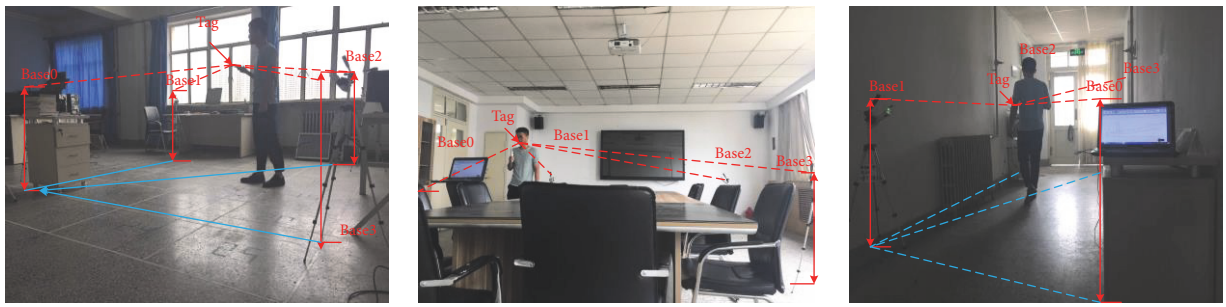


(a) Laboratory (b) Meeting-Room (c) corridor

Figure 3: Actual experimental environment diagram.

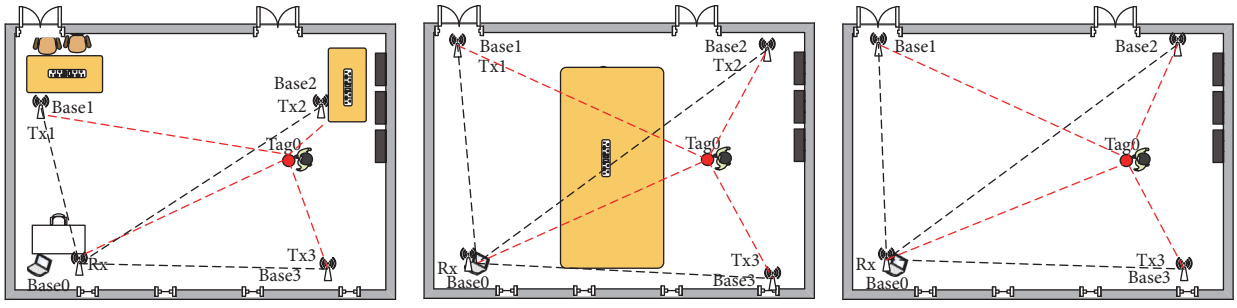


(a) Laboratory (b) Meeting-Room (c) corridor

Figure 4: Experimental environment plan.

### 4.2. Performance Analysis

*4.2.1. Human Influence on the Signal.* When a signal passes through a human body, a certain degree of attenuation occurs due to the blocking effect, and the signal forms a crawling wave. To express the effect of crawling waves intuitively, they are represented by a carrier signal and a modulated signal, as shown in Figure 6.

As shown by the carrier signal diagram in Figure 6(a), intuitively, signal propagation in the unmanned state is almost undisturbed, the carrier signal waveform tends to be flat and steady, the carrier signal spectrum has obvious regularity, and the signal approximates linear propagation; that is, the signal variations are weak—almost zero. The modulation signal diagram in Figure 6(b) shows that the signal is not as smooth as the carrier signal in the unmanned state in the experiment. However, the signal still shows some regularity, which confirms the presented concept of crawling waves. From Figure 6(b), it can be clearly seen that the law of crawling waves provides a theoretical basis for the subsequent Bayesian compressive sensing to eliminate the impact of crawling waves. Simultaneous modulation of the signal spectrum further confirms the method of this paper.

*4.2.2. Bayesian Algorithm Influence.* Under the premise of reducing the impact of human crawling waves, we studied the effects of Bayesian compressive sensing algorithm on signal transmission by analysing the modulated signal, as shown in Figure 7(a), and studied the signal recovery effect of Bayesian compressive sensing by evaluating the signal filtering effect, as shown in Figure 7(b).

From Figure 7(a), it can be seen that the Bayesian compressed sensing signal fusion integrates the crawling wave signal, and the obtained carrier signal is obviously much smoother. The impact of the crawling wave exists but decreases, indicating that the signal attenuation effect has been obtained and significantly improved. The filter gain response is shown in Figure 7(b). As the frequency increases, the filter gain tends to be stable and swings at -80 dB, which shows that the best effect of the gain response is -80 dB and that the corresponding signal frequency is 500 Hz.

From the Bayesian compressive sensing signal obtained as described above, the crawling wave is demodulated using two methods, as shown in Figure 8.

An analysis of Figure 8 shows that the envelope detection method and the synchronous product detection method both perform weak processing on the detected crawling wave

(a) Base station (b) Power supply (c) Network diagram (d) PC-side

Figure 5: Hardware testbed [17].

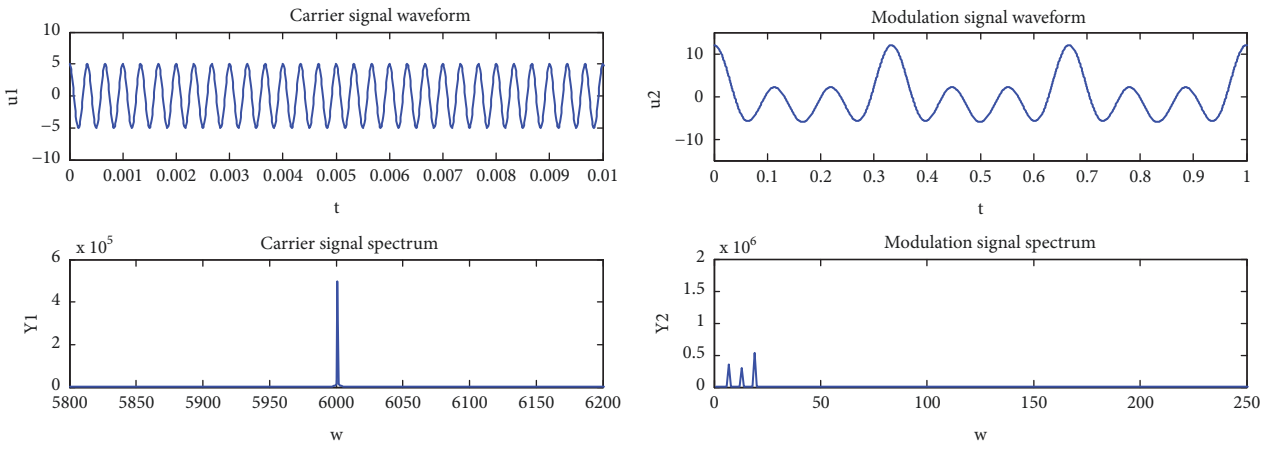


(a) Carrier signal (b) Modulation signal

Figure 6: Carrier signal and spectral density of carrier and modulation signals.

and reduce the debilitating effect of the signal. Comparing the waveform and spectral effects of the two methods, it is clear that the synchronous product detection method has more obvious effects on crawling waves: the debilitating effect of the signal after processing is significantly reduced. This result paves the way for the subsequent Bayesian compressive sensing to restore the signal strength.

The waveform and frequency of the signal before filtering are shown in Figure 9(a), and the gain response of the filter is shown in Figure 9(b).

By comparing the signal waveform before, after filtering and the spectrum change law, we can see that the scheduling value m plays a crucial role in signal modulation. The effect of the scheduling value m on the modulation of the crawling waves is shown in Figure 10.

As can be seen from the analysis in Figure 10, the present design accomplishes the modulation and demodulation of the AM signal and completes the time domain analysis of the AM signal. Through the Fourier transform, the spectrum of the modulated signal and the demodulated signal is obtained. As an illustration, we first set the amplitude of the carrier to 5, set the frequency to 3000, set the modulation to 0.1, modulate the useful signal, and obtain the corresponding waveform. Then, we use the two detection methods to solve the modulated waveform. For tuning, the two methods used are the envelope detection method and the synchronous product type detection method; together, the methods achieve the demodulation of the modulated wave. We also studied the effect of modulation on power and found that the ratio of the total power of the double sideband to the average total power gradually increased as the modulation degree increased.

At the end of these experiments, we studied the influence of the modulation degree on the waveform. When the modulation degree is zero, the modulation signal has no waveform, and as the modulation degree increases, the waveform becomes increasingly obvious. However, when the modulation degree exceeds 1, signal distortion occurs and unwanted waveforms appear. This indicates that the value of the modulation degree is between 0 and 1; it cannot be 0, and the maximum value is 1. A higher carrier frequency f can be selected, and the time sampling interval needs to be designed to be larger.

After completing the above signal processing, the influence of the crawling waves is successfully eliminated, and the signal weakness generated when the signal is blocked by the human body is effectively reduced.

*4.2.3. Impact of BCS-CW.* After exploring the effects of human body occlusion and the Bayesian algorithm on the signal transmission effect, this study performed experiments on the proposed algorithm combined with Bayesian compressive

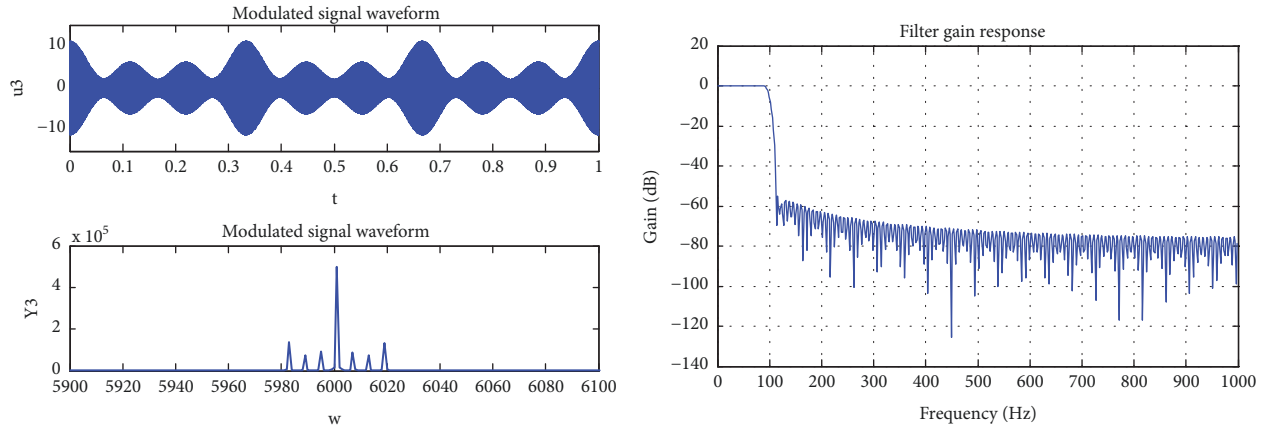


(a) Signal modulation (b) Filtering gain response

Figure 7: Carrier signal and spectral density for signal modulation and filtering gain response.

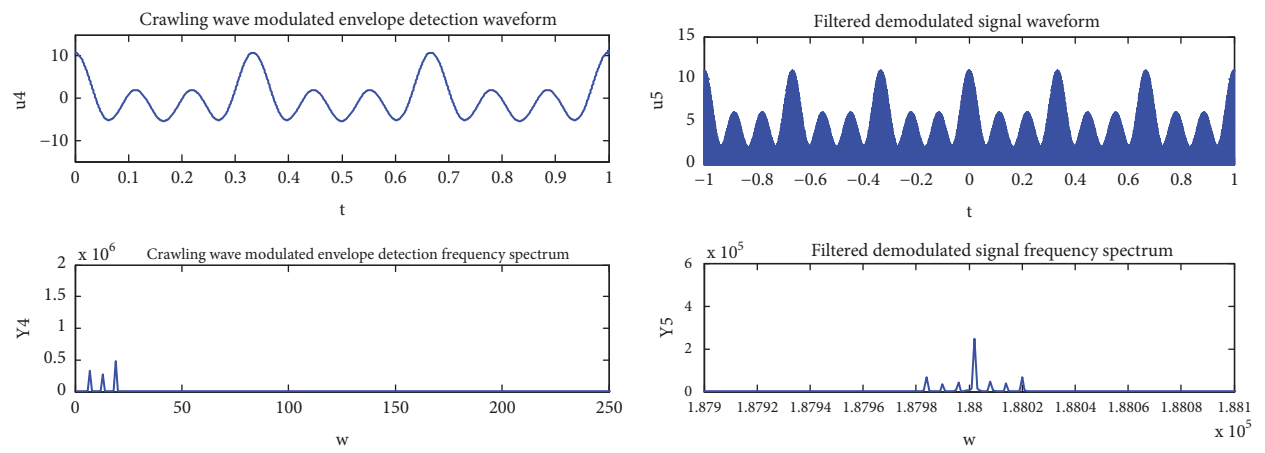


(a) Envelope detection (b) Synchronous product detection

Figure 8: Two ways of crawling wave demodulation.

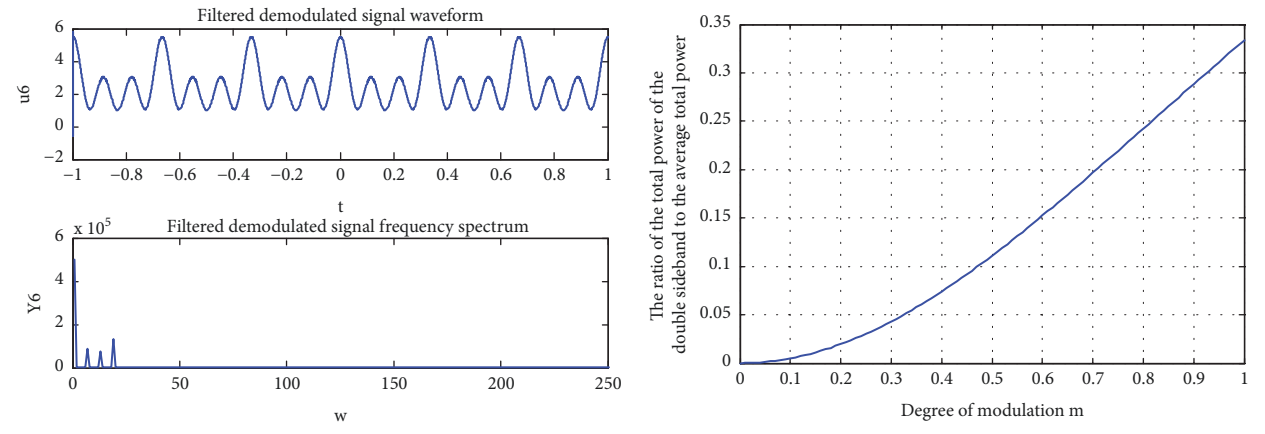


(a) The waveform and frequency before filtering (b) The gain response of the filter

Figure 9: The waveform and frequency of the signal.

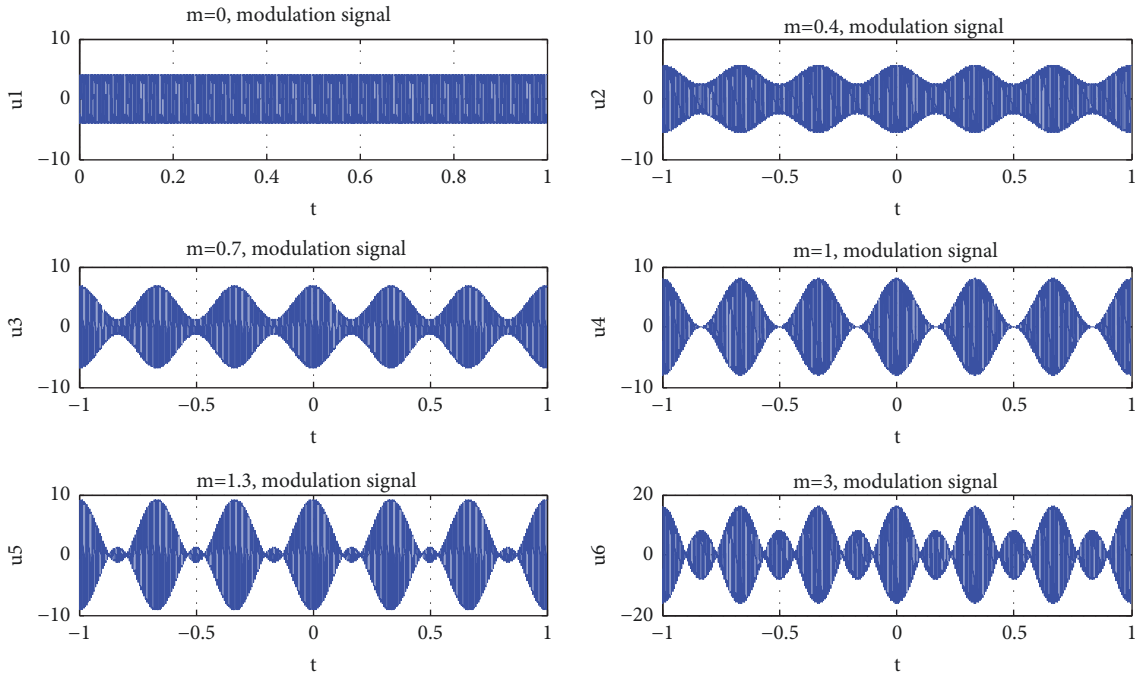


Figure 10: Effect of the scheduling value m on the modulation of crawling waves.

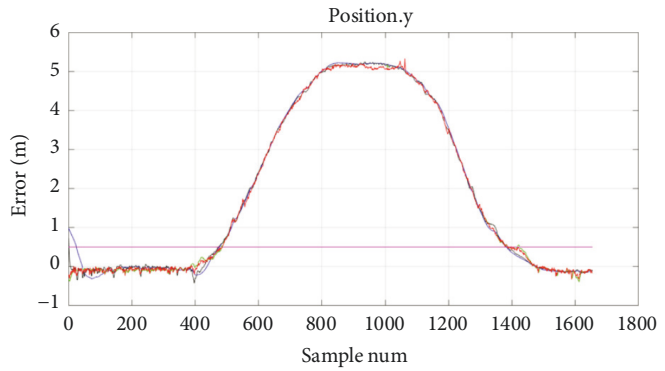


Figure 11: Error analysis.

sensing and obtained the transmission effect, positioning error, and sample numbers of the processed UWB signal. The relationship between these values is shown in Figure 11. The frequency state of the signal is shown in three-dimensional coordinates in Figure 12.

Figure 11 shows that as the number of samples increases, the positioning error changes. From the graph analysis, it can be seen that the maximum error is 5 m when the number of samples is between 800 and 1000, but the error tends toward 0 when the number of samples is between 0 and 400 or in excess of 1500. The ideal error situation occurs when the number of samples is between 1000 and 1500—the portion of the graph with a downward trend. This analysis shows that the number of samples has a certain influence on the positioning error.

The signal frequency diagrams on the x, y, and z-axes, respectively, are shown in Figure 12.

Figure 12 shows that the spectrum density of the UWB signals after Bayesian compressed sensing recovery is relatively stable, which indicates that the impact of crawling waves has largely been eliminated and demonstrates that Bayesian compressive sensing signal recovery has a significant effect on the elimination of crawling waves, providing support for further UWB accurate positioning. To verify the superiority of this method, we compared the algorithm with the Bayesian algorithm, the PCA algorithm, and the Kalman filter algorithm in both simple and complex environments, as shown in Figure 13.

From Figure 13, we can see that this algorithm significantly improves the localization accuracy compared to the other three methods in both simple and complex environments particularly in the latter. These results fully verify that the BCS-CW algorithm has a good recovery effect on

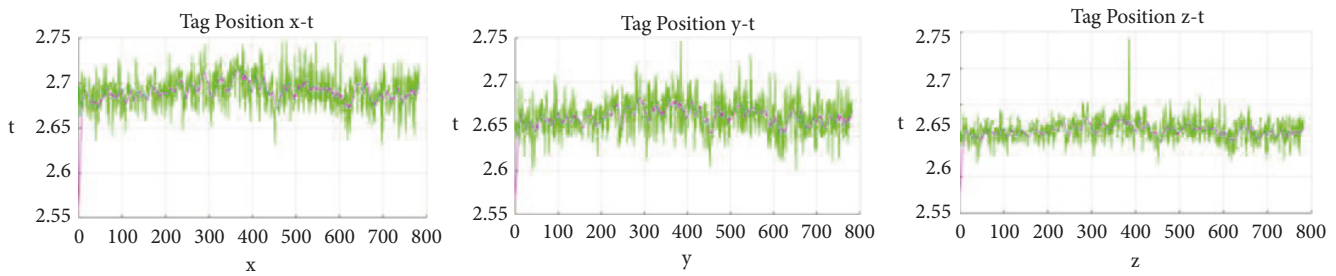


Figure 12: Signal frequency diagrams on the x, y, and z-axes.

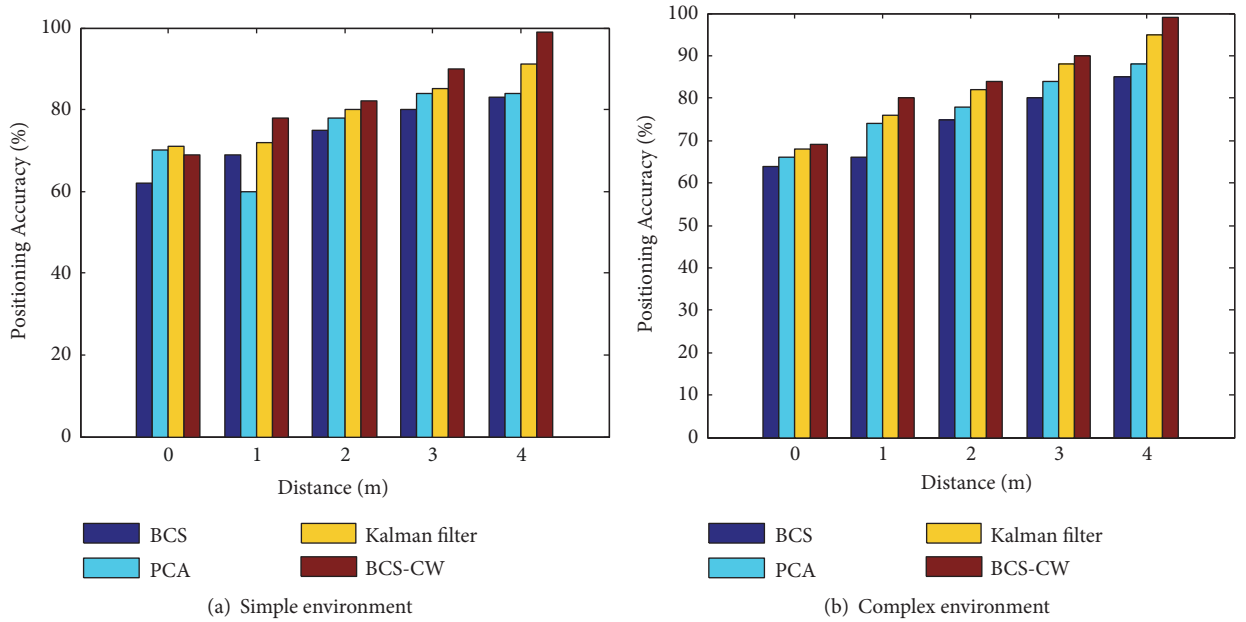


(a) Simple environment (b) Complex environment

Figure 13: Comparison of positioning accuracy in simple and complex environments.

UWB signals. It can be seen that the accuracy of BCS-CW is significantly higher than the PCA and Kalman filter algorithms. The BCS algorithm has the lowest accuracy. While ensuring high accuracy, the reliability and safety of the proposed algorithm are much higher than the other three methods. At the same time, the cost of the BCS-CW algorithm is relatively lower compared to other methods. In summary, the performance of the algorithm in this paper achieves a more accurate positioning and tracking effect.

## 5. Conclusions

In this paper, by combining the advantages of previous positioning methods, we propose a BCS-CW method that uses the local positioning system II-UWB LPS in conjunction with Bayesian compressive sensing to eliminate the effects of crawling waves under an environment with four base station tags. By analysing the transmission law of crawling waves on the human body, we obtained the main reason for the influence of human body occlusion on UWB signal transmission. Bayesian compressive sensing can recover the obtained UWB crawling wave signal; then, maximum likelihood estimation and the iterative approximation algorithm are combined to determine the tag's location. Finally, combined with actual environmental experiments, the proposed positioning accuracy after eliminating the impact of human crawling waves is greatly improved compared to other algorithms. The problem to be solved in future work is how to completely eliminate debilitated signals under human body occlusion. We plan to conduct further research in future work.

## Data Availability

This experiment was obtained in a real experimental environment, all data is actually available, and the relevant data has been described in the article.

## Conflicts of Interest

The authors declare that there are no conflicts of interest regarding the publication of this paper.

## Authors' Contributions

Li Beibei contributed to algorithm creation and to the analysis. As the supervisor of Hao Zhanjun, he proofread the paper several times and provided guidance throughout the entire manuscript preparation process. Dang Xiaochao contributed to the algorithms, the analysis, and the simulations and wrote the paper. Li Beibei and Hao Zhanjun revised the equations, helped write the introduction and related works sections, and critically revised the paper. All the authors have read and approved the final manuscript.

## Acknowledgments

This work was supported by the National Natural Science Foundation of China under Grant nos. 61762079 and 61662070; the Key Science and Technology Support Programme of Gansu Province under Grant nos. 1604FKCA097 and 17YF1GA015; and the Science and Technology Innovation Project of Gansu Province under Grant nos. 17CX2JA037 and 17CX2JA039.

## References

[1] Q. Zhihong, S. Dayang, and L. Victor, "Overview of wireless network positioning," *Chinese Journal of Computers*, vol. 39, no. 6, pp. 1237–1256, 2016.

[2] Y. Liu, Z. Yang, X. Wang, and L. Jian, "Location, localization, and localizability," *Journal of Computer Science and Technology*, vol. 25, no. 2, pp. 274–297, 2010.

[3] L. Ge, H. Zhang, H. Guo, and H. Wu, "High performance compressed sampling for OFDM-UWB systems," *China Communications*, vol. 14, no. 3, pp. 75–86, 2017.

[4] Z. Liang, J. Zang, X. Yang, X. Dong, and H. Song, "Low-density parity-check codes for noncoherent UWB communication systems," *China Communications*, vol. 14, no. 7, pp. 152–162, 2017.

[5] Y. Gu, Y. Chen, J. Liu, and X. Jiang, "Semi-supervised deep extreme learning machine for Wi-Fi based localization," *Neurocomputing*, vol. 166, pp. 282–293, 2015.

[6] C. Tsirmpas, A. Rompas, O. Fokou, and D. Koutsouris, "An indoor navigation system for visually impaired and elderly people based on radio frequency identification (RFID)," *Information Sciences*, vol. 320, pp. 288–305, 2015.

[7] Y. Fang, B. Wang, C. Sun, and V. Song, "A directional differential-fed uwb antenna with stable radiation pattern," *Journal of Nanjing University of Aeronautics and Astronautics (English Edition)*, vol. 33, no. 6, 2016.

[8] S. Liu, S. Wu, and Y. Li, "Application of Bayesian compressive sensing in IRUWB channel estimation," *China Communications*, vol. 14, no. 5, pp. 30–37, 2017.

[9] J. Peiquan, N. Wang, Z. Xiaoxiang et al., "Data management of mobile objects for indoor space," *Chinese Journal of Computers*, vol. 9, pp. 1777–1795, 2015.

[10] Z. Shujiang, Y. Jinsen, and H. Ping, "Node localization of wireless sensor networks based on weighted evaluation mechanism of linear parameters," *Computer Engineering*, vol. 43, no. 2, pp. 156–162, 2017.

[11] E. H. Jie, U. W. Ya-Nan, H. S. Duan et al., "Model of human body influence on UWB ranging error," *Journal of Communications*, 2017.

[12] Q. Zhou, C. Wu, J. Xing, J. Li, Z. Yang, and Q. Yang, "Wi-Dog: monitoring school violence with commodity WiFi devices," in *Wireless Algorithms, Systems, and Applications*, vol. 10251 of *Lecture Notes in Computer Science*, pp. 47–59, Springer International Publishing, Cham, Switzerland, 2017.

[13] D. Xuefang and W. Qi, "Wi-Fi indoor location algorithm based on improved support vector machine," *Computer Engineering and Applications*, vol. 52, no. 6, pp. 90–93, 2016.

[14] K. Wei and W. Lenan, "Positioning and tracking algorithm based on non-linear error direct estimation," *Signal Processing*, vol. 26, no. 12, pp. 1858–1863, 2010.

[15] X. Xu, Z. Zhang, W. Li, and H. Tan, "Research on pedestrian detection method based on the intersection with fixed camera," in *Proceedings of the International Symposium on Computational Intelligence and Design*, pp. 311–314, IEEE, Hangzhou, China, December 2016.

[16] L. Gong, W. Yang, Z. Zhou et al., "An adaptive wireless passive human detection via fine-grained physical layer information," *Ad Hoc Networks*, vol. 38, pp. 38–50, 2016.

[17] Z. Hao, B. Li, and X. Dang, "A method for improving UWB indoor positioning," *Mathematical Problems in Engineering*, vol. 2018, Article ID 8740872, 17 pages, 2018.

[18] R. Zhou, X. Lu, P. Zhao, and J. Chen, "Device-free presence detection and localization with SVM and CSI fingerprinting," *IEEE Sensors Journal*, vol. 17, no. 23, pp. 7990–7999, 2017.

[19] J. Wang, H. Jiang, J. Xiong et al., "LiFS: low human effort, device-free localization with fine-grained subcarrier information," in *Proceedings of the 22nd Annual International Conference on Mobile Computing and Networking*, pp. 243–256, ACM, New York, NY, USA, October 2016.

[20] Y. Xie, Z. Li, and M. Li, "Precise power delay profiling with commodity WiFi," in *Proceedings of the 21st Annual International Conference on Mobile Computing and Networking*, pp. 53–64, ACM, Paris, France, September 2015.

[21] J. Li and X. Ji, "A novel method of Wi-Fi indoor localization based on channel state information," in *Proceedings of the 8th International Conference on Wireless Communications Signal Processing (WCSP)*, pp. 1–5, IEEE, Yangzhou, China, 2016.

[22] Y. Zhang, J. Huang, and K. Xu, "WLAN indoor positioning method based on PCA-LSSVR algorithm," *Journal of Instrumentation and Instrument*, vol. 36, no. 2, pp. 408–414, 2015.

[23] Z. Liang, J. Zang, X. Yang, X. Dong, and H. Song, "Integration interval determination and decision threshold optimization for improved TRPC-UWB communication systems," *China Communications*, vol. 14, no. 5, pp. 185–192, 2017.

[24] M. F. Abdulhalim and B. A. A. Attea, "Multi-layer genetic algorithm for maximum disjoint reliable set covers problem in wireless sensor networks," *Wireless Personal Communications*, vol. 80, no. 1, pp. 203–227, 2014.

[25] A. Ahmad, E. Serpedin, H. Nounou, and M. Nounou, "Joint node localization and time-varying clock synchronization in wireless sensor networks," *IEEE Transactions on Wireless Communications*, vol. 12, no. 10, pp. 5322–5333, 2013.

[26] Z. Wu, Q. Xu, J. Li, C. Fu, Q. Xuan, and Y. Xiang, "Passive indoor localization based on CSI and naive bayes classification," *IEEE Transactions on Systems, Man, and Cybernetics: Systems*, vol. 48, no. 9, pp. 1566–1577, 2018.

[27] S. Shi, S. Sigg, and Y. Ji, "Probabilistic fingerprinting based passive device-free localization from channel state information," in *Proceedings of the 2016 IEEE 83rd Vehicular Technology Conference (VTC Spring)*, pp. 1–5, IEEE, Nanjing, China, May 2016.

[28] X. Wang, L. Gao, and S. Mao, "BiLoc: bi-modal deep learning for indoor localization with commodity 5GHz wifi," *IEEE Access*, vol. 5, pp. 4209–4220, 2017.

[29] X. Li, F. Guo, L. Yang, and M. Zhang, "Improved solution for geolocating a known altitude source using TDOA and FDOA under random sensor location errors," *IEEE Electronics Letters*, vol. 54, no. 9, pp. 597–599, 2018.

[30] Y. Fang, B. Wang, C. Sun, Z. Song, and S. Wang, "A directional differential-fed UWB antenna with stable radiation pattern," *Journal of Nanjing University of Aeronautics and Astronautics: English Version*, vol. 33, no. 6, pp. 747–753, 2016.

[31] Y. Chen and E. J. Candes, "The projected power method: an efficient algorithm for joint alignment from pairwise differences," *Communications on Pure and Applied Mathematics*, vol. 71, no. 8, pp. 1648–1714, 2018.